Available online at www.HEFJournal.org

ISSN: 2785-2997

Journal of
Human, Earth, and Future

Vol. 3, No. 2, June, 2022

Molecular Dynamics Simulation to Investigate the Effect of Al_2O_3 Doping and Compression on the Structural Properties of Aluminium Silicate Glass

Pham Huu Kien [1], Thonchit Monesaykham [1], Giap Thi Thuy Trang [1*]

[1] *Thai Nguyen University of Education, No. 20 Luong Ngoc Quyen, Thai Nguyen, Viet Nam*

Received 19 March 2022; Revised 11 May 2022; Accepted 26 May 2022; Published 01 June 2022

Abstract

In this paper, we have performed molecular dynamics simulation to investigate the effect of Al_2O_3 doping and compression on the structural properties of aluminium silicate (AS2) glass. The structural properties are examined via TO_x units, OT_y linkages, the average bond angle distributions, order parameters, and cluster function. The result shows that the network structure of AS2 is mainly built by TO_x units and OT_y linkages (T = Si or Al, x = 3-7, y = 2-4). We found that in AS2 glass, the subnet structure performed by the perfect SiO_x units is not transfigured. Meanwhile, the AlO_x units are significantly distorted. The structural organization of the SiO4-network in AS2 glass is not dependent on Al_2O_3 doping. Moreover, the degree of structural homogenous significantly depends on compression. In the range of 15–25 GPa, the structural homogenous of AS2 is caused by the mobility of all atoms, tightly related to the glass-glass transition. Our work is expected to support finding the AS2 compositions that can produce hard and damage-tolerant glasses in the higher pressure region.

Keywords: Al_2O_3 Doping; Heterogeneous; Glass-Glass Transition; The Fastest Atoms; The Slowest Atoms.

1. Introduction

Aluminium Silicate (AS2) glass plays an important role in several geochemical applications, such as low-melting glassy materials, radiation shielding materials, photonics and the electronic industry. As we know, AS2 is another multi-component oxide system with a network-forming structure [1-9]. Many experimental techniques such as nuclear magnetic resonance, X-ray scattering, infrared, and Raman spectroscopy [10–14] found evidence for structural units, such as 3-fold coordinated by O atoms and 5- and 6-fold coordinated by Si (Al) atoms that are not found in pure SiO_2, unless one considers SiO_2 glass at a high-pressure region. With low Al_2O_3 concentrations, the Al atoms in AS2 glass are mainly 4-fold coordinated by O atoms. From large angle X-ray scattering, IR and Raman spectroscopies, Urata et al. [15] showed that the average *T*–O distances do not depend on the concentration of Al_2O_3 doping. The common neighbour (CN) of AS2 glass is about 4. A homogeneous AS2 network is formed, where the number of SiO_4 tetrahedra gradually decreases with increasing Al_2O_3 doping. From NMR spectroscopic, Sen et al. [16], Weber et al. [17] showed that the structure of homogeneous AS2 glass with 0.4 to up to 12.0 wt% Al_2O_3 contains a mixture of 4-, 5-, and 6-fold coordinated by Al sites (Al^{IV}, Al^{V}, and Al^{VI}). The average Al coordination increases from 4.57 to 4.73 as

* Corresponding author: tranggtt@tnue.edu.vn

http://dx.doi.org/10. 28991/HEF-2022-03-02-03

the fraction of octahedral Al increases with alumina content. The coordination polyhedra of a significant fraction of the Al^{VI} sites in these glasses are found to be unusually distorted, similar to that in the case of crystalline Al_2SiO_5 polymorphs. The ^{17}O NMR spectra showed the presence of three types of O sites, Si-O-Al^{V}, Si-O-Al^{IV}, and Si-O-Si, in these glasses. Analysis of the neutron and X-ray structure factors yields an average bond angle of 125^0 between an Al ion and the adjoining cation via a bridging O. They proposed that the structure of the glass is a "transition state" between the Al-rich liquid and the equilibrium Mullite phase that is dominated by 4- and 6-coordinated by Al ions, respectively.

The simulation technique provides more details about the structural properties of AS2 glass at atomic levels [18-26]. Using MD simulation, Fleiderer et al. [27] reported that the structure of AS2 is that the Al and Si atoms are mainly 4-fold coordinated by O. Unlike SiO_4, AlO_4 units are linked to each other by triclusters (OAl_3 linkages) and edge-sharing AlO_4 tetrahedra. They suggested that a micro-segregation happens due to an Al-rich region percolating via the Si–O network. Hoang et al. [28] showed evidence of DH in high-density AS2. They found that the fastest/slowest atoms tend to form clusters, depending on temperature and their mean cluster size. According to Liu et al. [29] and Benitez et al. [30], the average Si-Si and Al-Si CN decrease while those in Si-Al and Al-Al CN increase with the increase of Al_2O_3 doping. The bridging O, classified into Si-O-Si, Al-O-Al and Si-O-Al, is preferentially localized in Si-O-Al. The Al-O-Al/Al is much smaller than the Al-O-Si/Al, indicating that the Al-O-Si bond is more stable than the Al-O-Al bond. Si atoms coordinated to four O atoms are independent of the chemical composition. The number of O atoms coordinated to two decreased as the amount of Al_2O_3 doping was increased, while the opposite occurred for O atoms coordinated to three. As the amount of Al_2O_3 doping increased, Al atoms coordinated to four O atoms were reduced, whereas Al atoms coordinated to five O atoms were increased. Winkler et al. [31] reported that the structure of AS2 is that of a disordered tetrahedral network. The packing of AlO_4 tetrahedra is significantly different from that of SiO_4 tetrahedra in that Al is complicated with a relatively high probability in small-membered rings and in triclusters in which an O atom is surrounded by 4 Si (Al) atoms. They found that the system shows a micro-phase separation in which the Al-rich region percolates through the SiO_2 network on larger length scales. In addition, in *ab* initio simulation, molecular orbital calculations confirmed the existence of "*triclusters*" in AS2 [32-35].

Although the structural features of AS2 glass and melts has been studied for a long time. Up to now, the local environment of Si, O, Al atoms is still in debate. Especially, the characteristic of topologic of AlO_x units in Al_2O_3 doping is also not considered yet. In this paper, we use MD simulation, visualization of MD data to investigate the effect of Al_2O_3 doping and compression on the structural properties of AS2 glass. The goal of this work is to clarify the effect of Al_2O_3 doping, glass-glass phase transition, and the nature of structural heterogeneity in the AS2 glass.

2. Research Methodology

A series of AS2 models has been performed by molecular dynamics (MD) simulation. In this work, the constructed model consists of 3003 atoms (546 Si, 546 Al, 1911 O atoms) in the range of 0-60 GPa and temperatures of 600 K. The pair-wise additive potential with Coulombic interaction and Born-Mayer repulsion is used to construct AS2 models. The detailed information of these potential parameters can be found by Hong et al. [24] and Hoang [28]. The Verlet algorithm is applied to integrate the equations of motion, here time step of 1.46 *fs*. Firstly, all atoms of configuration (model) are randomly placed in a simulation cube box; its size is corresponding to the density of the AS2 glass system. This model is equilibrated at a temperature of 6000 K about 2×10^5 time steps. After, a model is cooled down to different temperatures 3000, 2000, 1500, 1000, and final 600 K, with the rate of 10^{-11} K/s. Then it is compressed to a different pressures (5, 10, 15, 20, 25, 30, 35, 40, 45, 50, 55, 60 GPa) and relaxed for 2×10^6 time steps. In this way, we formed two pure Al_2O_3 and SiO_2 at ambient pressure and temperature of 300 K to compare to AS2 model. A consequent long relaxation (5×10^7 time steps) for each of the models has been completed in the NPT ensemble to obtain a good equilibrium model. To improve the statistics, the partial RDF, CN distribution, and bond angle distributions (BAD) are calculated by averaging over 2000 configurations separated by 20 time steps. Figure 1 shows the flowchart of the research methodology.

3. Analysis

3.1. The Effect of Al_2O_3 Doping on the Structure of AS2 Glass

Firstly, the reliability of constructed models is determined via some structural parameters such as the pair RDF of all atomic pairs, average bond angle distributions (BAD), and average coordination number (CN). Our obtained parameters are also compared with experimental and simulation data. As shown in Table 1, the simulation results are close to simulated data by Pfleiderer et al. [27] and Winkler et al. [31] and consist with experimental data from Ohira et al. [6], Okuno et al. [36]. Figure 2 displays visual of arrangement of AS2 model at ambient pressure, temperature of 600 K. Here, one can see the TO_3, TO_4, TO_5, TO_6, TO_7 units, as well as the OT_2, OT_3 and OT_4 linkages. As seen, TO_x units connect together via common O atoms to form TO_x and OT_y (x = 3-7, y = 2-4) clusters.

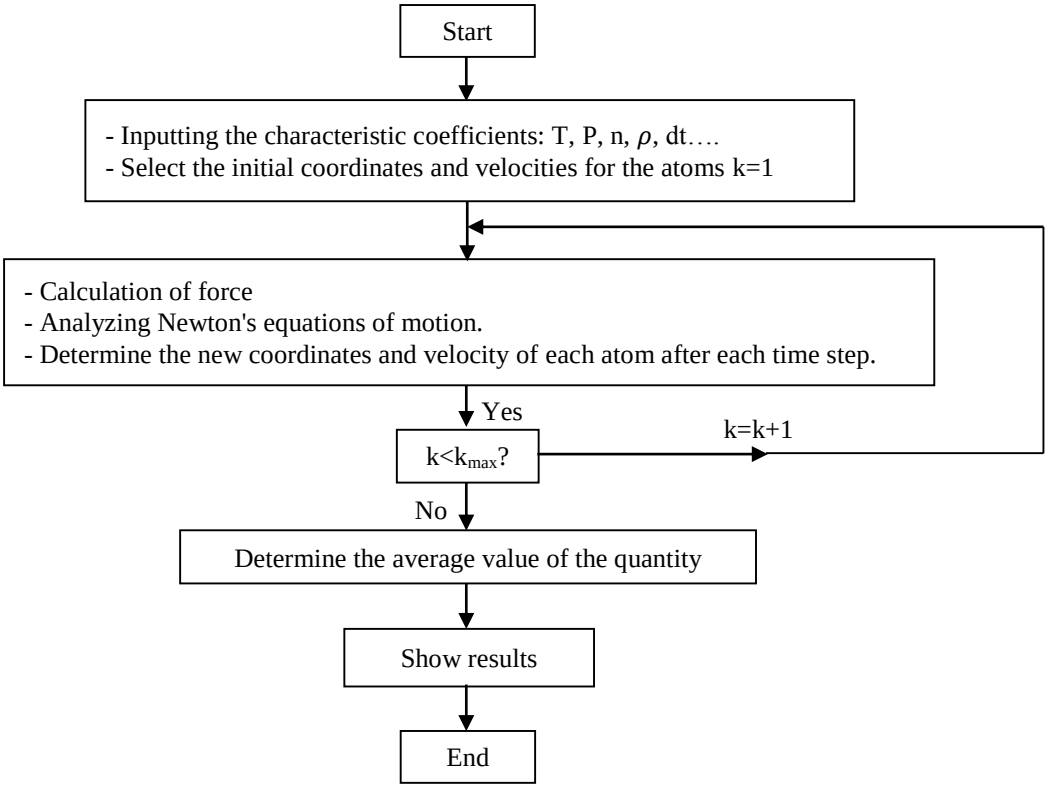

Figure 1. Flowchart of molecular dynamics simulation method

Table 1. The structural characteristics of AS2 glass: r_{X-Y} - the position and height of the first peak of RDFs $G_{X-Y}(r)$, CN_{X-Y} - the average coordination number; θ - position of the highest peak of BAD

	Present Study			Sim. [27, 31]	Exp.	
ρ, g/cm	**2.43**	**3.78**	**4.14**	**2.60**	**0 GPa [6]**	**131 GPa [36]**
r_{Si-O}, Å	1.60±0.02	1.66±0.02	1.68±0.02	1.65	1.59	1.64
r_{Al-O}, Å	1.66±0.02	1.76±0.02	1.76±0.02	1.67	1.70	1.81
r_{O-O}, Å	2.60±0.02	2.50±0.02	2.44±0.02	2.68	-	-
r_{Si-Si}, Å	3.18±0.02	3.16±0.02	3.12±0.02	3.15	-	-
r_{Al-Si}, Å	3.18±0.02	3.12±0.02	3.04±0.02	3.23	-	-
r_{Al-Al}, Å	3.16±0.02	3.06±0.02	2.98±0.02	3.15	-	-
CN_{Si-O}	4.09±0.05	5.24±0.05	5.57±0.05	4.48	4.01	~ 6.00
CN_{Al-O}	4.34±0.05	5.00±0.05	5.17±0.05	4.29	4.01	~ 6.00
$<\theta_{O-Si-O}>$	108°±4°	90°; 168°±2⁰	90°; 168°±2⁰	108.2	-	-
$<\theta_{O-Al-O}>$	78.5°; 107°±4°	79°; 164°±2⁰	79°; 164°±2⁰	85.8°; 109.8°	-	-

Figure 3 shows the pair RDFs of AS2 model at ambient pressure, temperature of 600 K. These pairs RDFs exhibit a disordered structure. The first peak of the $G_{Si-O}(r)$ locates at 1.62 ± 0.02 Å. This peak is contributed from the Si-O bond distance of SiO_4 and SiO_5 units. For AlO_y units, the first peak of the $G_{Al-O}(r)$, contributed from the Al–O bond distance of AlO_4, AlO_5 and AlO_6 units, it locates at 1.68 ± 0.02 Å. However, the average Al–O bond distance of AlO_4, AlO_5 and AlO_6 units are 1.66 ± 0.02 Å, 1.72 ± 0.02 Å and 1.74 ± 0.02 Å, respectively. The first peak of the $G_{O-O}(r)$ locates at 2.62 ± 0.02 Å, while that of the $G_{Si-Si}(r)$ locates at 3.18 ± 0.02 Å. Meanwhile, the first peak of the $G_{Al-Al}(r)$ splits slightly into two sub-peaks which big one locates at 3.12 ± 0.02 Å and small one locates at 2.72 ± 0.02 Å. For the Si-Al pair, the first peak of the $G_{Si-Al}(r)$ locates at 3.20 ± 0.02 Å. These data are consistent with the experimental data [6, 10-14] and calculated results [20-27, 31], this can also be see Table 1.

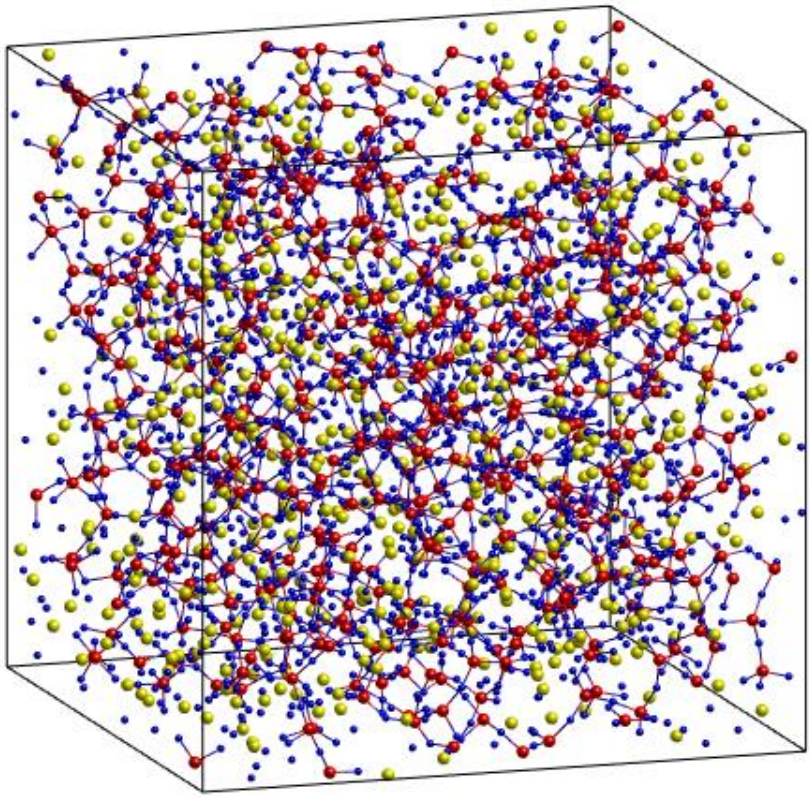

Figure 2. Snapshots of the atomic arrangement of AS2 model at ambient pressure, the temperature of 600 K. Here Si, Al, and O atoms are in red, yellow, and blue color, respectively

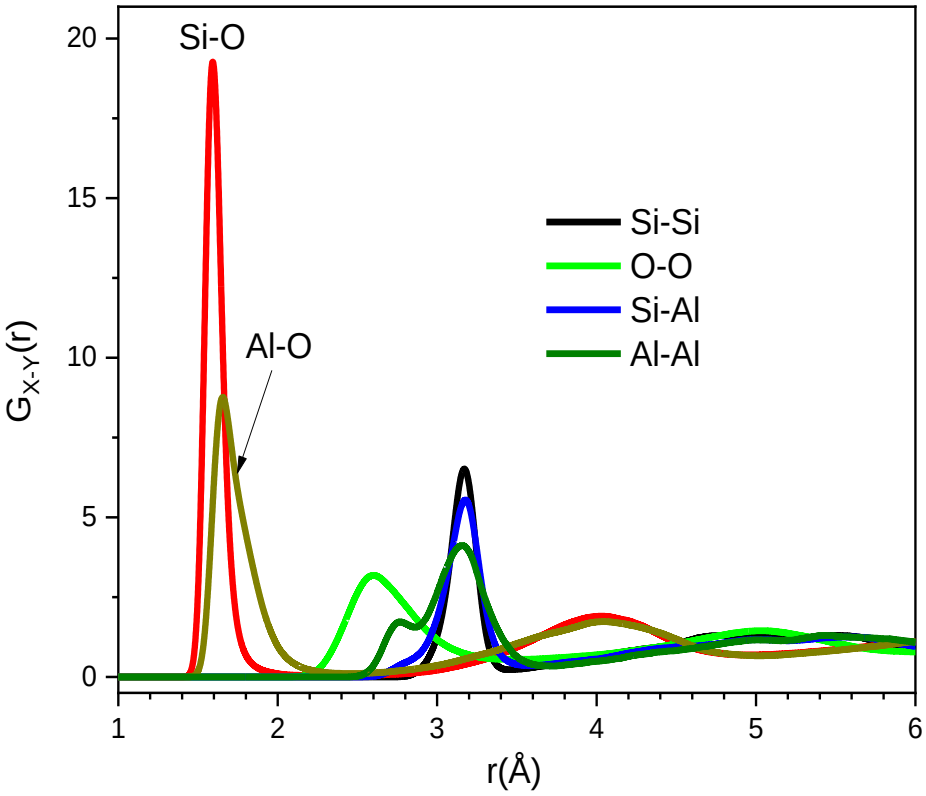

Figure 3. The pair RDFs of Si—O, Al—O, O—O, Si—Si, Al—Al, and Si—Al pairs of AS2 model at ambient pressure and 600

Figure 4 shows the $G_{T\text{-}O}(r)$ RDFs at ambient pressures, temperature of 600 K. As seem, the location of the first peak, as well as the shape of the pair RDFs Si-O in pure SiO_2 and AS2 glasses, are almost not dependent on the Al_2O_3 doping. They are located at 2.62 ± 0.02 Å, and the height of the pair RDFs Si-O are 20.0 and 22.5 Å, respectively. These values are rather good agreement with the ones reported by [1-8, 12-14, 18-23]. In contrast, the location of the first peak, as well as the shape of the pair RDFs Al-O in pure Al_2O_3 and AS2 glasses differs significantly, i.e., the location of the first peak of the pair RDFs Al-O in pure Al_2O_3 glass is 1.72 ± 0.02 Å, and it is 1.68 ± 0.02 Å in the case of AS2 glass. In other words, the pair RDFs Al-O is significantly dependent on the Al_2O_3 doping in AS2 glass.

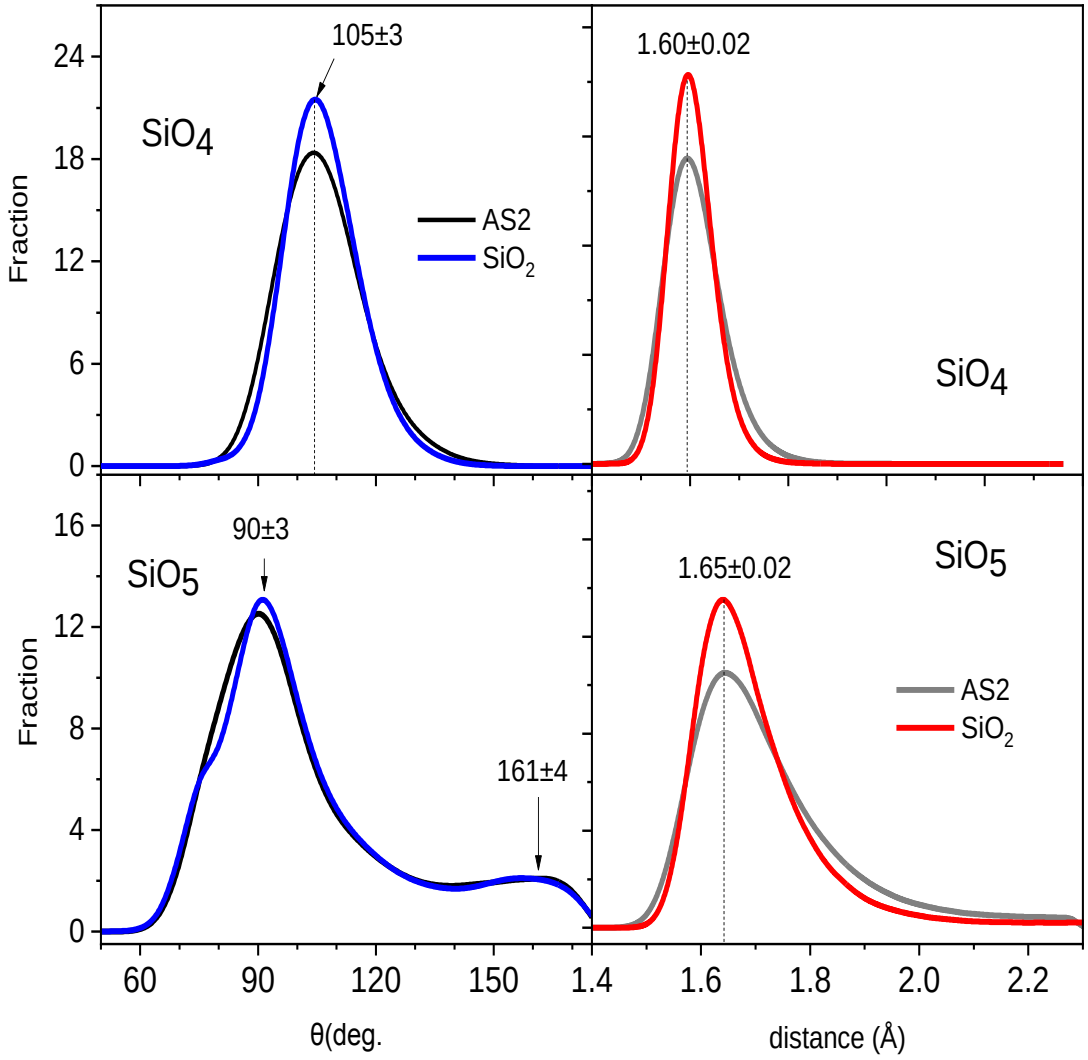

Figure 4. The comparison to the pair RDFs Si—O, Al—O between the pure SiO_2, Al_2O_3, and AS2 glasses

Detail information about basic TO_x units is inferred from the bond distances distribution and DABs. Figure 5 displays the $\theta_{O\text{-}Si\text{-}O}$ bond angle and Si-O bond distances distribution in SiO_4, SiO_5 units pure SiO_2 and AS2 glasses. As we known, ideal tetrahedron the angle of O-Si-O and Si-O bond distance, are equal to 109.7° and 1.62 Å, respectively. In our models the $<\theta_{O\text{-}Si\text{-}O}>$ angle distribution and Si-O bond distance of SiO_4 have peak at 105° and 1.60 ± 0.02 Å that indicated distorted tetrahedral network structure. In the case of SiO_5 units both curves for $\theta_{O\text{-}Si\text{-}O}$ DAB has a main peak centered at 90° and second peak which occurred near 155°. The both curves for Si-O bond distance distribution has a main peak centered at 1.65 ± 0.02 Å. These values are rather good agreement with the ones reported by Yang et al. [37], Mozzi and Warren [38], Pettifer et al. [39]. It is interesting that these distributions are almost unchanged with Al_2O_3 doping.

Figure 6 displays the $\theta_{O\text{-}Al\text{-}O}$ bond angle and Al-O bond distance distribution in AlO_4, AlO_5, and AlO_6 units in pure Al_2O_3 and AS2 glasses. Comparing to pure Al_2O_3 and AS2 glass, it can be seen that most graph has a main peak differed significantly. Namely, the partial $\theta_{O\text{-}Al\text{-}O}$ BAD in AlO_4, AlO_5, and AlO_6 units in pure Al_2O_3 glass have a main peak at around 105, 86, and 85° and a shoulder at around 165° corresponding to AlO_5, and AlO_6, they are 103, 92 and 87° and a shoulder at around 155° and 168° in AS2. Further, the Al-O bond distances have a main peak at around 1.72, 178, 1.82 Å corresponding to the AlO_4, AlO_5, and AlO_6 units in pure Al_2O_3 glass, they are at around 1.74, 183, 1.84 Å in AS2 glass. This means that the basic units AlO_x in AS2 are strongly distorted.

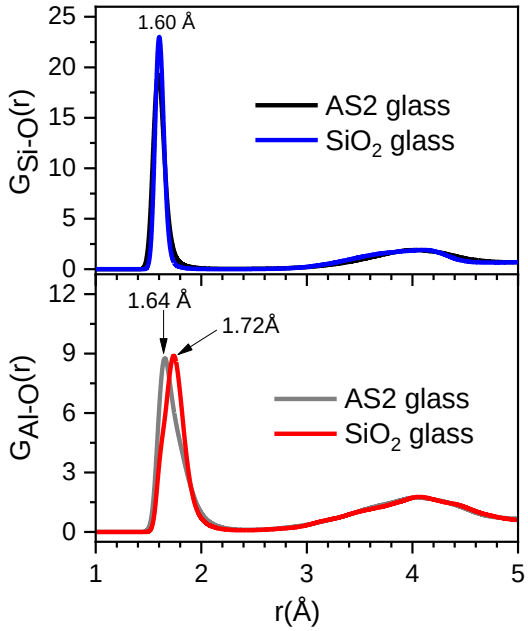

Figure 5. The θ_{O-Si-O} bond angle and Si—O bond distance distribution in SiO_4, SiO_5 units of the pure SiO_2 and AS2 glasses

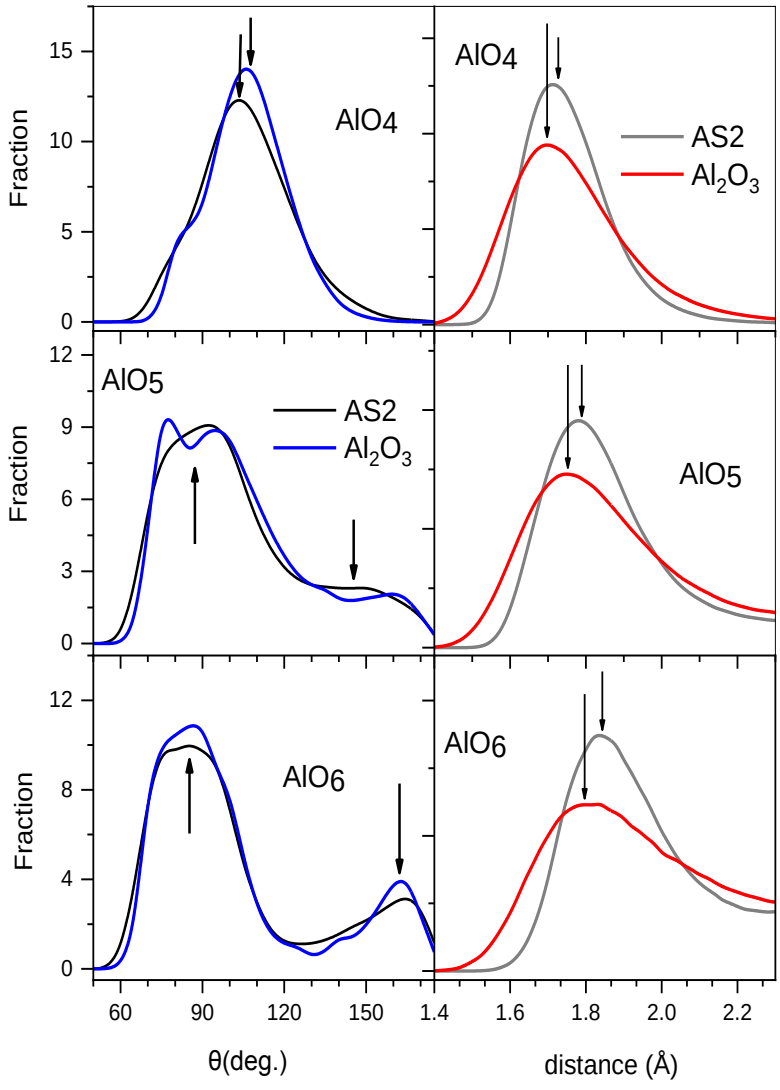

Figure 6. The θ_{O-Al-O} bond angle and Al—O bond distance distribution in AlO_4, AlO_5, and AlO_6 units for pure Al_2O_3 and AS2 glasses. An arrow presents the position of the main peak on curves that shows the difference between an idea and distorted AlO_4, AlO_5, and AlO_6 units.

From the above analysis, we can conclude that the network structure of AS2 glass at ambient pressure, and temperature of 600 K is built by TO_x (mainly SiO_4) units, in which the SiO_x units are ideal tetrahedron; in contrast, the AlO_x units are significantly distorted. The transfiguration of AlO_x units in Al_2O_3 doping can be explained as follows. The Si-O bond lengths in SiO_x units are shorter than the Al-O in AlO_x units. The Coulomb repulsion between Si^{4+} and O^{2-} is larger than Al^{3+} and O^{2-}. Therefore, Al-O links are weaker than Si-O links, this leads to the network structure formed by SiO_x units is more steady-state in AS2 glass. In other words, the network structure of SiO_2 in AS is not dependent the Al_2O_3 doping.

3.2. The Effect of Compression on the Structure of AS2 Glass

Figure 7 shows the evolution of average *T*-O, O-*T* (*T* is Si or Al) coordination number (CN) and the order parameter η as a function of pressure in AS2 model. As seen in Figure 6A, under compression, the average *T*-O CN tends to increase from 4-fold (at ambient pressure) to 6-fold (at high pressure). Meanwhile, the O-*T* CN increases from 2.31 to 3.28. In the range of 0–6 GPa, the *T*-O coordination increases strongly, most of the structural units are TO_4, In the range of 6-24 GPa, the *T*-O CN gradual increases with pressure, the structure of AS2 mainly comprises the TO_4, TO_5 units and some the AlO_6. In the range of 24-60 GPa, the *T*-O coordination increases slightly, the structure of AS2 mainly comprises the TO_6 units and some the TO_5, AlO_6, AlO_7 units. The change of average *T*-O CN is similar to one of average O-*T* CN. We can conclude that the structure of AS2 comprises two phases/states: LD and HD phases. The LD phase is formed from TO_4 units that are linked to each other via OT_2 linkages. This means that the LD phase is characteristic of TO_4 units and OT_2 linkages. The HD phase is formed from TO_5, TO_6 and AlO_7 units that are linked to each other mainly via OT_3 linkages. Under compression, there is a gradual transition from LD phase to HD phase corresponding to the gradual structural transition from TO_4 to TO_6 and some AlO_7 units. So, in the range of 0-60 GPa, the structure of AS2 glass comprises both two LD and HD phases. At a certain density, most of the linkages between TO_x units are OT_2 OT_3 and some OAl_4. The phase transition points are determined as seen in Figure 7. One can be shown that the curve for fraction C_{TO5} intersects the one for C_{TO4} and C_{TO6} at 6 ± 0.5 and 24 ± 0.5 GPa, respectively.

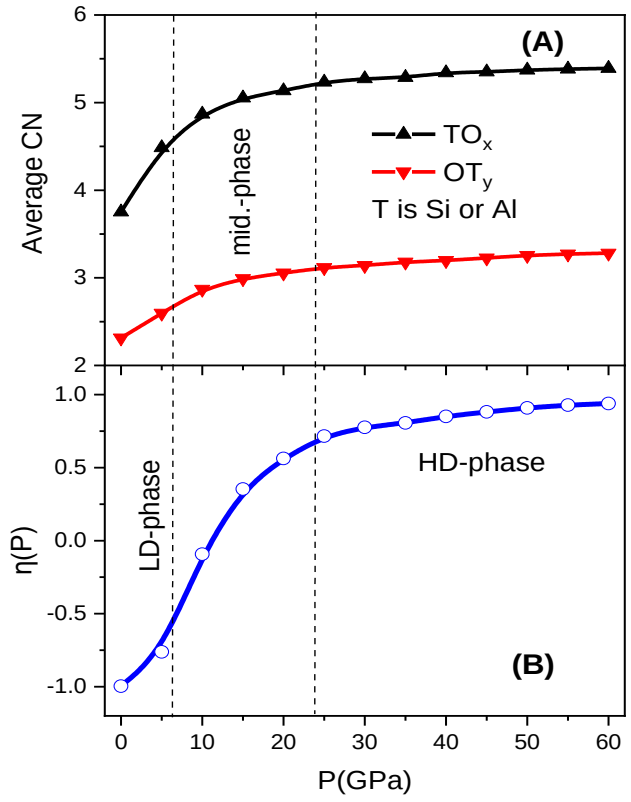

Figure 7. Panel A displays the evolution of average coordination number (CN) as a function of pressure. Panel B shows the pressure dependence of the order parameter η of the AS2 model at different pressures

According to Figure 8, largest fraction C_x for 0-6, 6-24, 24-60 GPa intervals is fraction C_{TO4}, C_{TO5} and C_{TO6}, respectively. This implies that large phases for those intervals are LD-phase, LD- and HD-phases, and HD-phases, respectively. Thus, the structure of AS2 glass undergoes through three pressure regions, corresponding with existence of LD-phase, LD-, and HD-phases implied the polymorphism of AS2 glasses.

Next, in order to get some insights into the glass-glass transition in AS2 glass, we have used the order parameter:

$$\eta(P) = \frac{n_6 - n_4}{n_6 + n_4} \quad (1)$$

Here, n_4 and n_6 are the numbers of 4-fold and 6-fold coordinated T atoms to oxygen. Note that if $\eta(P) = -1$ there is no 6-fold coordination in the system and analogously if $\eta(P) = 1$ there is no 4-fold coordination. The order parameter is plotted in Figure 6B as a function of pressure and no abrupt change from a tetrahedral to an octahedral order has been found due to the existence of the 5-fold coordinated unit TO_5 in the system. This means that the first-order nature of the glass-glass transition in AS2 glass is not found clearly.

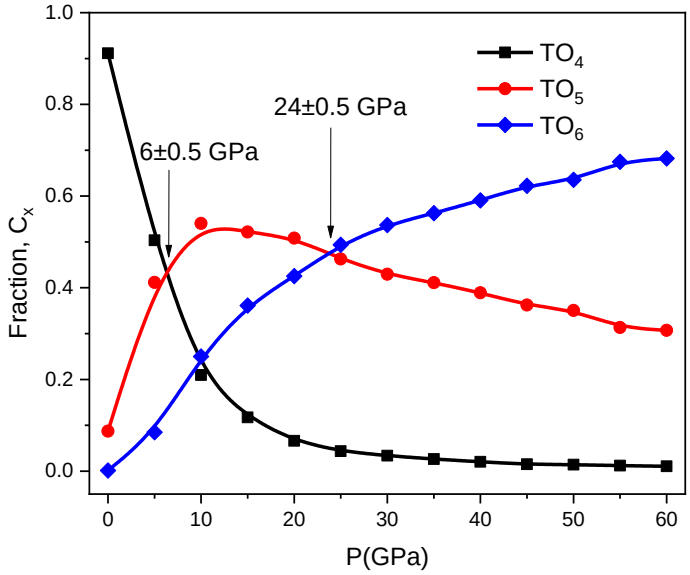

Figure 8. Pressure dependence of C_{TO4}, C_{TO5} and C_{TO6} fractions. Here, the black arrows present the phase transition points

Figure 9 shows the total $\theta_{O\text{-}Si\text{-}O}$, $\theta_{O\text{-}Al\text{-}O}$ BAD in AS2 model at different pressures. From Figure 8 (left), as seen, total $\theta_{O\text{-}Si\text{-}O}$ BAD strongly changes with pressure: the main peak slightly shifts to a lower angle and its height decreases with increasing pressure, at a pressure of 5 GPa the main peak tends to split into two peaks, a small peak located at 168° ± 4°. Figure 9 (right) shows the total $\theta_{O\text{-}Al\text{-}O}$ BAD also significantly varies. At 0 GPa, its main peak is located at 103° ± 4°. The main peak slightly shifts to a lower angle and its height decreases with increasing pressure, at a pressure of 15 GPa appears the second sub-peaks located around of 162° ± 4°. With increasing pressure, the height of two sub-peaks strongly increases. In the high-pressure regions, the total $\theta_{O\text{-}Al\text{-}O}$ and $\theta_{O\text{-}Si\text{-}O}$ BADs appears the second sub-peak which also results in forming HD-phase in AS2 glass. This result is rather good agreement with the ones reported in experimental and simulation works [3-12, 18, 27, 30-36].

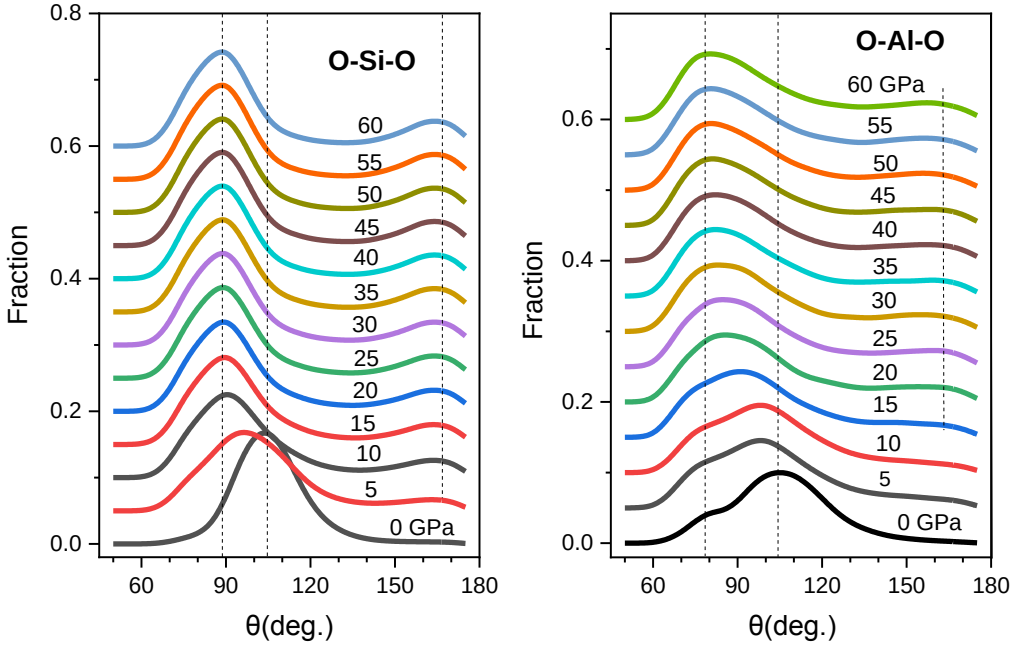

Figure 9. The total $\theta_{O\text{–}Si\text{–}O}$ and $\theta_{O\text{–}Al\text{–}O}$ bond angles distribution in AS2 model at different pressures

Next, we have determined the cluster-function (CL-function) for sets of the fastest and slowest atoms (SMA and SIMA). The number of atoms in these sets is 1000 which is about 33% of total atoms. The atoms of SMA and SIMA are determined from their positions in the starting configuration and configuration at t = 80 ps. An atom belongs to SMA or SIMA, if its MSD is respectively larger or smaller than that of other atoms not belonging to the given set. Thus the atoms of SMA and SIMA represent respectively the fastest and slowest atoms. Here, we call for simplicity the atom of SMA and SIMA, fastest and slowest atom. The CL-function $f_{CL}(r)$ for SMA and SIMA have been determined for configurations at time t = 80ps is plotted in Figure 10. As seen, below 10 GPa, the $f_{CL}(r)$ for SIMA drops fast from 1.5 to 2.0 Å, while for SMA it largely decreases in the interval between 2.5 and 3.5 Å. Moreover, the $f_{CL}(r)$ for SIMA varies gradually as r > 2.0 Å. The fast drop of $f_{CL}(r)$ of SIMA is caused by that the slowest atoms form larger LC-clusters by small r. In the range of 15-20 GPa, the CL-function $f_{CL}(r)$ for SMA and SIMA are rather close to other, they drop fast from 2.0 to 3.0Å. Beyond 25 GPa, the $f_{CL}(r)$ for SIMA drops fast from 1.5 to 2.0 Å, while for SMA it largely decreases in the interval between 2.5 and 4.0 Å. Moreover the $f_{CL}(r)$ for SIMA varies very gradually as r > 2.0 Å.

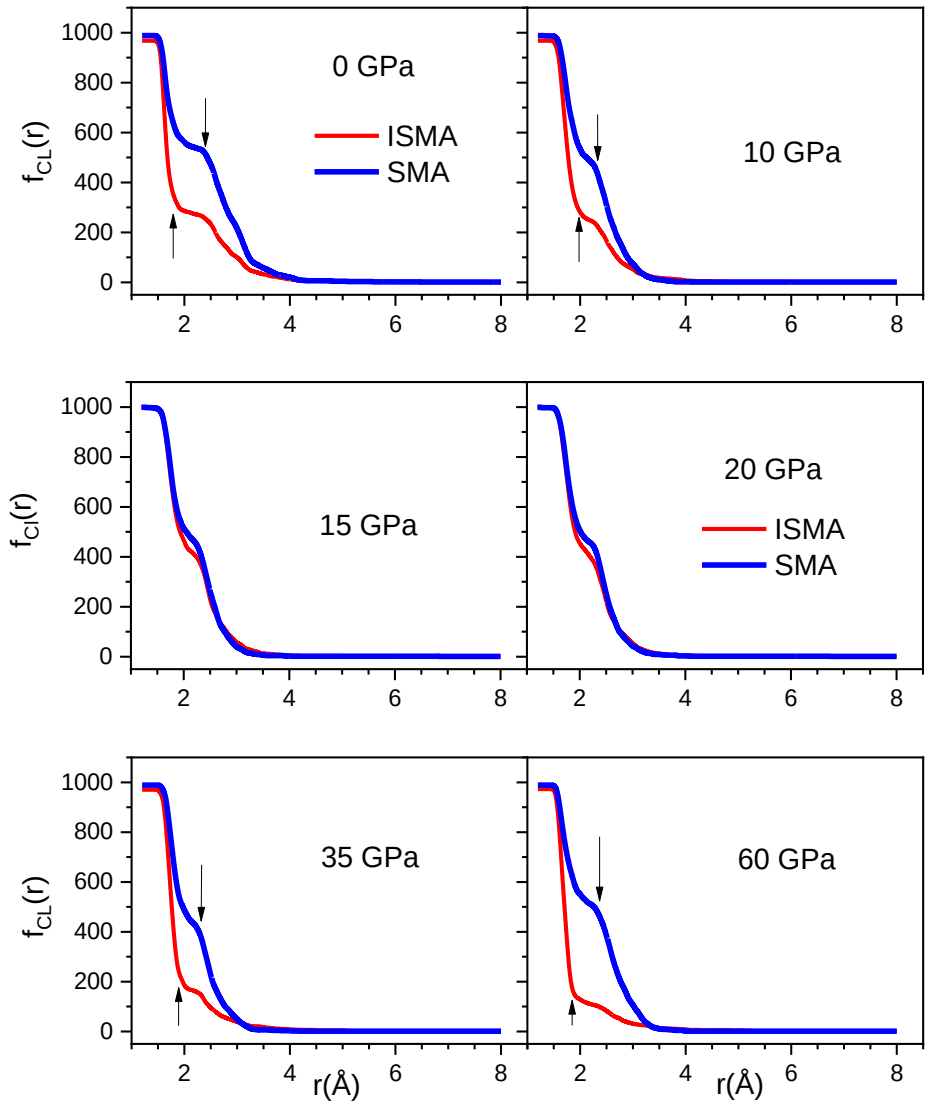

Figure 10. The CL-function for atoms of SMA and SIMA in the AS2 configurations at time t = 80 ps, at different pressures. Here, the black arrows denote the position that the curves drop the fastest

Finally, to check heterogeneous of the micro-structure for AS2 glass we visual randomly the 300 fastest and 300 slowest atoms in the model. Figure 11 shows the snapshots of the fastest and slowest atoms in AS2 glass at different pressures. At 0, 40 GPa, it can be seen that both the fastest and slowest atoms tend to form clusters, and the distributions are not uniform. It demonstrates that the dynamics/microstructure of atoms in the glass state is heterogeneous. In addition, the fastest and slowest atoms tend to segregate. In contrast, at 15 GPa, both the fastest and slowest atom distributions are rather uniform. As seen, O atoms are the fastest in all atoms and the mobility of all atoms increases in the following order: Si, Al, and O atoms. This result good consists of the picture the Figure 11.

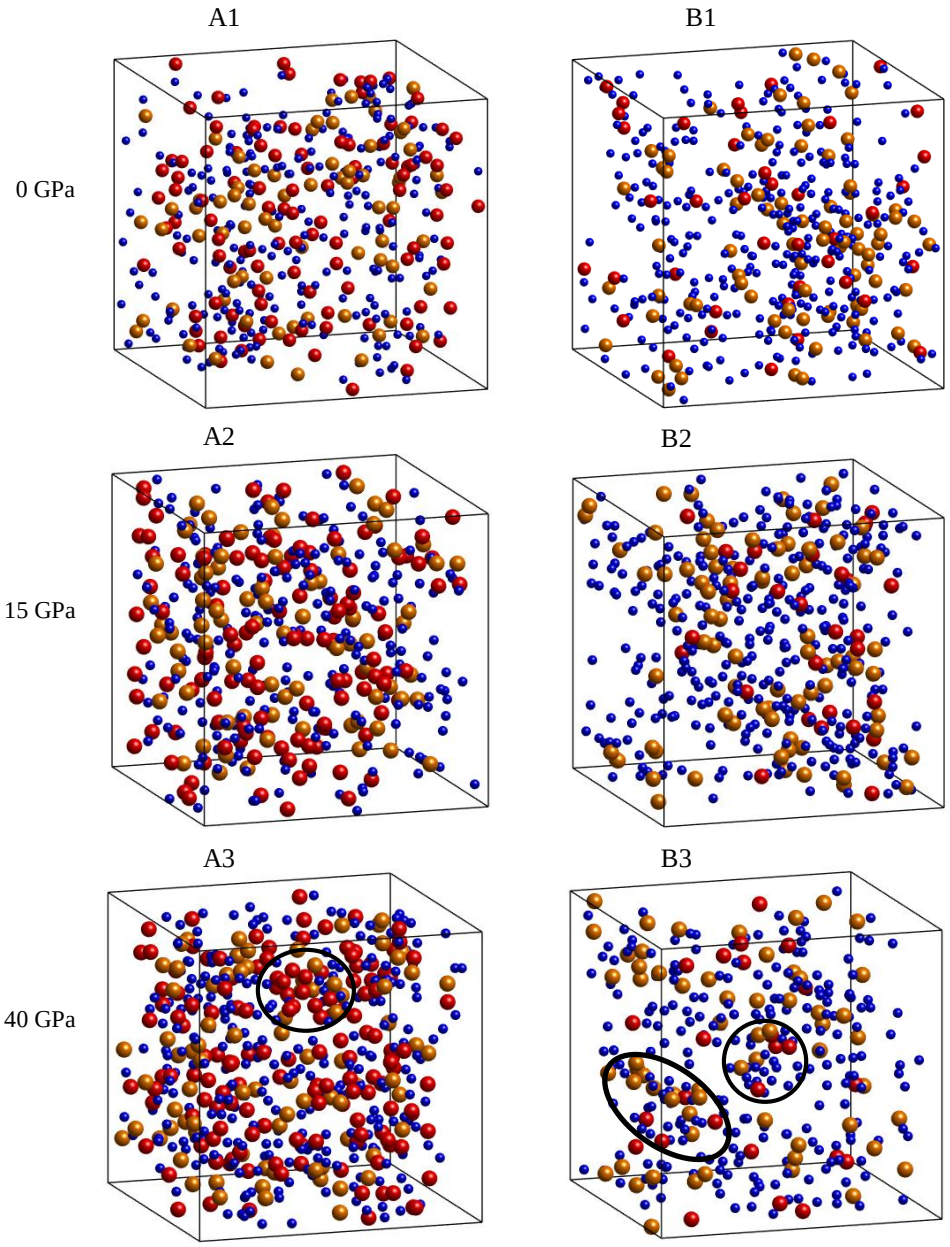

Figure 11. Snapshot of the positions of the slowest (A1, A2, A3) and fastest (B1, B2, B3) atoms for the AS2 models at 0, 15 and 40 GPa. Here, the red, blue and dark-yellow spheres represent the Si, O and Al atoms, respectively. The black-solid circles denote the clustering of the fastest and slowest atoms.

From the above analysis, we can conclude that the network structure of AS2 is uniform in the range of 15–25 GPa. In contrast, the network structure of AS2 is heterogeneous in the range of 0–15 and 25–60 GPa. In other words, the degree of heterogeneous significantly depends on compression. This has not been considered yet in [3, 26, 40, 41]. The structural uniformity of AS2 is caused by the mobility of all atoms in the range of 15–25 GPa, relating to the glass–glass transition. With the pressure increasing, the local density fluctuations lead to the formation of the spatial dynamical regions in a system that form the structural heterogeneous.

4. Conclusions

A MD simulation of the effect of Al_2O_3 doping and compression on the structural properties of AS2 glass has been successfully performed. Following results are obtained:

- The network structure of AS2 glass comprises basic structural units such as SiO_x and AlO_y. In the range of 0–6 GPa, AS2 mainly comprises SiO_4, AlO_3, and AlO_4. In the range of 6–24 GPa, AS2 mainly comprises SiO_4, SiO_5, AlO_4, and AlO_5. Beyond 24 GPa, most of the SiO_x and AlO_y units are SiO_5, SiO_6, AlO_6, and some AlO_7 units. Under compression, the average *T*-O and O-*T* CNs increase. This leads to a transition from LD-phase to HD-phase, corresponding to the gradual structural transition from TO_4 to TO_6 and some AlO_7 units.

- We found that the network structure of SiO_2 in AS2 is not dependent on Al_2O_3 doping; meanwhile, the AlO_x units belonging to Al_2O_3 doping are significantly distorted. Moreover, the network structure of AS2 is homogenous in the range of 15–25 GPa. In contrast, it is heterogeneous in the range of 0–15 GPa and beyond 25 GPa. The degree of structural heterogeneous in AS2 glass significantly depends on compression. The structural homogenous of AS2 resulted from the mobility of all atoms in the range of 15-25 GPa which tight correlates to glass-glass transition. This result is a calculation of our simulation that can be tested by scattering experimental approaches.

5. Declarations

5.1. Author Contributions

Conceptualization, P.H.K.; methodology, G.T.T.T.; software, P.H.K. and T.M.; validation G.T.T.T.; formal analysis, P.H.K.; investigation, G.T.T.T.; resources, G.T.T.T.; data curation, T.M.; writing—original draft preparation, G.T.T.T. and T.M.; writing—review and editing, P.H.K. and G.T.T.T.; supervision, T.M.; project administration, P.H.K.; funding acquisition, P.H.K. All authors have read and agreed to the published version of the manuscript.

5.2. Data Availability Statement

The data presented in this study are available in article.

5.3. Funding

This research is funded by Thainguyen University under grant number ĐH2022-TN04-02.

5.4. Institutional Review Board Statement

Not Applicable.

5.5. Informed Consent Statement

Not Applicable.

5.6. Declaration of Competing Interest

The authors declare that there is no conflict of interests regarding the publication of this manuscript. In addition, the ethical issues, including plagiarism, informed consent, misconduct, data fabrication and/or falsification, double publication and/or submission, and redundancies have been completely observed by the authors.

6. References

[1] Watson, E. B. (1981). Diffusion in magmas at depth in the Earth: The effects of pressure and dissolved H2O. Earth and Planetary Science Letters, 52(2), 291–301. doi:10.1016/0012-821X(81)90184-9.

[2] Totea, A. M., Dorin, I., Laity, P. R., Sabin, J., Conway, B. R., Waters, L., & Asare-Addo, K. (2020). A molecular understanding of magnesium aluminium silicate – drug, drug – polymer, magnesium aluminium silicate – polymer nanocomposite complex interactions in modulating drug release: Towards zero order release. European Journal of Pharmaceutics and Biopharmaceutics, 154, 270–282. doi:10.1016/j.ejpb.2020.07.027.

[3] Vinh, L. T., Hung, P. K., Ba Van, T., & Hong, N. V. (2020). Computer simulation of local microstructure and dynamics in aluminum-silicate melt. Modelling and Simulation in Materials Science and Engineering, 28(3). doi:10.1088/1361-651X/ab6ec6.

[4] Zhou, Q., Shi, Y., Deng, B., Neuefeind, J., & Bauchy, M. (2021). Experimental method to quantify the ring size distribution in silicate glasses and simulation validation thereof. Science Advances, 7(28), 1761. doi:10.1126/sciadv.abh1761.

[5] Shih, Y. T., Sundararaman, S., & Huang, L. (2020). Structural origin of the anomalous density maximum in silica and alkali silicate glasses. Journal of the American Ceramic Society, 103(7), 3942–3953. doi:10.1111/jace.16850.

[6] Ohira, I., Kono, Y., Shibazaki, Y., Kenney-Benson, C., Masuno, A., & Shen, G. (2019). Ultrahigh pressure structural changes in a 60 mol. % Al2O3-40 mol. % SiO2 glass. Geochemical Perspectives Letters, 10, 41–45. doi:10.7185/geochemlet.1913.

[7] Le Losq, C., Neuville, D. R., Florian, P., Henderson, G. S., & Massiot, D. (2014). The role of Al3+ on rheology and structural changes in sodium silicate and aluminosilicate glasses and melts. Geochimica et Cosmochimica Acta, 126, 495–517. doi:10.1016/j.gca.2013.11.010.

[8] Rosales-Sosa, G. A., Masuno, A., Higo, Y., & Inoue, H. Crack-resistant Al2O3–SiO2 glasses. Scientific Reports, 6(1), 1–7.

[9] Zheng, K., Zhang, Z., Yang, F., & Sridhar, S. (2012). Molecular dynamics study of the structural properties of calcium aluminosilicate slags with varying Al2O3/SiO2 ratios. ISIJ International, 52(3), 342–349. doi:10.2355/isijinternational.52.342.

[10] Wilding, M. C., & Benmore, C. J. (2006). Structure of glasses and melts. Reviews in Mineralogy and Geochemistry, 63(1), 275–311. doi:10.2138/rmg.2006.63.12.

[11] Greaves, G. N. (1988). EXAFS and the structure of catalysts. Catalysis Today, 2(5), 581–584. doi:10.1016/0920-5861(88)85021-1.

[12] Stebbins, J. F., & Xu, Z. (1997). NMR evidence for excess non-bridging oxygen in an aluminosilicate glass. Nature, 390(6655), 60–62. doi:10.1038/36312.

[13] Lee, S. K., & Stebbins, J. F. (2000). The Structure of Aluminosilicate Glasses: High-Resolution 17O and 27Al MAS and 3QMAS NMR Study. Journal of Physical Chemistry B, 104(17), 4091–4100. doi:10.1021/jp994273w.

[14] Pask, J. A. (1996). Importance of Starting Materials on Reactions and Phase Equilibria in the Al2O3-SiO2 System. Journal of the European Ceramic Society, 16(2 SPEC. ISS.), 101–108. doi:10.1016/0955-2219(95)00147-6.

[15] Urata, S., Nakamura, N., Tada, T., & Hosono, H. (2021). Molecular dynamics study on the co-doping effect of Al2O3 and fluorine to reduce Rayleigh scattering of silica glass. Journal of the American Ceramic Society, 104(10), 5001 – 5015. doi:10.1111/jace.17774.

[16] Sen, S., & Youngman, R. E. (2004). High-resolution multinuclear NMR structural study of binary aluminosilicate and other related glasses. Journal of Physical Chemistry B, 108(23), 7557–7564. doi:10.1021/jp031348u.

[17] Weber, R., Sen, S., Youngman, R. E., Hart, R. T., & Benmore, C. J. (2008). Structure of high alumina content A12O3-SiO 2 composition glasses. Journal of Physical Chemistry B, 112(51), 16726–16733. doi:10.1021/jp807964u.

[18] Atila, A., Ghardi, E. M., Ouaskit, S., & Hasnaoui, A. (2019). Atomistic insights into the impact of charge balancing cations on the structure and properties of aluminosilicate glasses. Physical Review B, 100(14). doi:10.1103/PhysRevB.100.144109.

[19] Karki, B. B., Ghosh, D. B., & Bajgain, S. K. (2018). Simulation of silicate melts under pressure. Magmas under Pressure: Advances in High-Pressure Experiments on Structure and Properties of Melts, 419–453. doi:10.1016/B978-0-12-811301-1.00016-2.

[20] Charpentier, T., Okhotnikov, K., Novikov, A. N., Hennet, L., Fischer, H. E., Neuville, D. R., & Florian, P. (2018). Structure of Strontium Aluminosilicate Glasses from Molecular Dynamics Simulation, Neutron Diffraction, and Nuclear Magnetic Resonance Studies. Journal of Physical Chemistry B, 122(41), 9567–9583. doi:10.1021/acs.jpcb.8b05721.

[21] Drewitt, J. W. E., Jahn, S., Sanloup, C., De Grouchy, C., Garbarino, G., & Hennet, L. (2015). Development of chemical and topological structure in aluminosilicate liquids and glasses at high pressure. Journal of Physics Condensed Matter, 27(10). doi:10.1088/0953-8984/27/10/105103.

[22] Wang, Y., Sakamaki, T., Skinner, L. B., Jing, Z., Yu, T., Kono, Y., Park, C., Shen, G., Rivers, M. L., & Sutton, S. R. (2014). Atomistic insight into viscosity and density of silicate melts under pressure. Nature Communications, 5(1), 1–10. doi:10.1038/ncomms4241.

[23] Luo, J., Vargheese, K. D., Tandia, A., Harris, J. T., & Mauro, J. C. (2016). Structural origin of intrinsic ductility in binary aluminosilicate glasses. Journal of Non-Crystalline Solids, 452, 297–306. doi:10.1016/j.jnoncrysol.2016.09.010.

[24] Hong, N. V., Yen, N. V., Lan, M. T., & Hung, P. K. (2014). Coordination and polyamorphism of aluminium silicate under high pressure: Insight from analysis and visualization of molecular dynamics data. Canadian Journal of Physics, 92(12), 1573–1580. doi:10.1139/cjp-2014-0042.

[25] Lodesani, F., Menziani, M. C., Hijiya, H., Takato, Y., Urata, S., & Pedone, A. (2020). Structural origins of the Mixed Alkali Effect in Alkali Aluminosilicate Glasses: Molecular Dynamics Study and its Assessment. Scientific Reports, 10(1), 1–18. doi:10.1038/s41598-020-59875-7.

[26] Van, T. B., Hung, P. K., Vinh, L. T., Yen, N. V., Ha, N. T. T., & San, L. T. (2021). Domain structure, microscopic segregation and dynamics heterogeneity in alumina-silicate liquid. Journal of Non-Crystalline Solids, 552(120457). doi:10.1016/j.jnoncrysol.2020.120457.

[27] Pfleiderer, P., Horbach, J., & Binder, K. (2006). Structure and transport properties of amorphous aluminium silicates: Computer simulation studies. Chemical Geology, 229(1–3), 186–197. doi:10.1016/j.chemgeo.2006.01.020.

[28] Hoang, V. (2007). Dynamical heterogeneity and diffusion in high-density Al2O3·2SiO2 melts. Physica B: Condensed Matter, 400(1–2), 278–286. doi:10.1016/j.physb.2007.07.023.

[29] Liu, Y., Bai, C., Lv, X., & Wei, R. (2015). Molecular Dynamics Simulation on the Influence of Al2O3 on the Slag Structure at 1873 K. Materials Today: Proceedings, 2, S453–S459. doi:10.1016/j.matpr.2015.05.061.

[30] Benitez, T., Rivas Murillo, J. S., de Ligny, D., Travitzky, N., Novaes de Oliveira, A. P., & Hotza, D. (2020). Modeling the effect of the addition of alumina on structural characteristics and tensile deformation response of aluminosilicate glasses. Ceramics International, 46(13), 21657–21666. doi:10.1016/j.ceramint.2020.05.273.

[31] Winkler, A., Horbach, J., Kob, W., & Binder, K. (2004). Structure and diffusion in amorphous aluminum silicate: A molecular dynamics computer simulation. Journal of Chemical Physics, 120(1), 384–393. doi:10.1063/1.1630562.

[32] Kubicki, J. D., & Toplis, M. J. (2002). Molecular orbital calculations on aluminosilicate tricluster molecules: Implications for the structure of aluminosilicate glasses. American Mineralogist, 87(5–6), 668–678. doi:10.2138/am-2002-5-609.

[33] Toplis, M. J., Dingwell, D. B., Hess, K. U., & Lenci, T. (1997). Viscosity, fragility, and configurational entropy of melts along the join SiO2-NaAlSiO4. American Mineralogist, 82(9–10), 979–990. doi:10.2138/am-1997-9-1014.

[34] Toplis, M. J., Dingwell, D. B., & Lenci, T. (1997). Peraluminous viscosity maxima in Na2O-Al2O3-SiO2 liquids: The role of triclusters in tectosilicate melts. Geochimica et Cosmochimica Acta, 61(13), 2605–2612. doi:10.1016/S0016-7037(97)00126-9.

[35] Xue, X., & Kanzaki, M. (1999). NMR Characteristics of Possible Oxygen Sites in Aluminosilicate Glasses and Melts: An ab Initio Study. Journal of Physical Chemistry B, 103(49), 10816–10830. doi:10.1021/jp992108a.

[36] Okuno, M., Zotov, N., Schmücker, M., & Schneider, H. (2005). Structure of SiO2-Al2O3 glasses: Combined X-ray diffraction, IR and Raman studies. Journal of Non-Crystalline Solids, 351(12–13), 1032–1038. doi:10.1016/j.jnoncrysol.2005.01.014.

[37] Yang, F., Zhou, W., Zhu, R., Dai, G., Wang, W., Wang, W., … Wang, Z. (2021). Synergistic effects of amorphous porous materials and anhydrous Na2CO3 on the performance of bricks with high municipal sewage sludge content. Journal of Cleaner Production, 280, 124338. doi:10.1016/j.jclepro.2020.124338

[38] Mozzi, R. L., & Warren, B. E. (1970). The structure of vitreous boron oxide. Journal of Applied Crystallography, 3(4), 251–257. doi:10.1107/s0021889870006143

[39] Pettifer, R. F., Dupree, R., Farnan, I., & Sternberg, U. (1988). NMR determinations of SiOSi bond angle distributions in silica. Journal of Non-Crystalline Solids, 106(1–3), 408–412. doi:10.1016/0022-3093(88)90299-2.

[40] Kien, P. H., Yen, N. V., & Hong, N. V. (2020). The study of structure and dynamics of liquid Al2O3·2SiO2 at higher temperatures. Phase Transitions, 93(2), 274–286. doi:10.1080/01411594.2020.1716354.

[41] Hung, P. K., Vinh, L. T., Van, T. B., Hong, N. V., & Yen, N. V. (2017). Insight into dynamics and microstructure of aluminum-silicate melts from molecular dynamics simulation. Journal of Non-Crystalline Solids, 462, 1–9. doi:10.1016/j.jnoncrysol.2017.02.003.